Topics in Catalysis Vol. 39, Nos. 1–2, September 2006 (© 2006)
DOI: 10.1007/s11244-006-0043-4

Characterization and catalytic activity of unpromoted and alkali (earth)-promoted Au/Al_2O_3 catalysts for low-temperature CO oxidation

A.C. Gluhoi[a], X. Tang[a], P. Marginean[b], and B.E. Nieuwenhuys[a,*],

[a]*Department of Heterogeneous Catalysis and Surface Chemistry, Leiden Institute of Chemistry, Leiden University, P.O. Box 9502, 2300 RA Leiden, The Netherlands*

[b]*National Institute for Research and Development of Isotopic and Molecular Technologies, P.O. Box 700 R-3400 Cluj-Napoca 5, Romania*

Various unpromoted and alkali (earth) promoted gold catalysts were characterized by means of XRD, HRTEM, DR/UV–Vis and TPR. Based on the results we conclude that metallic Au is the active species in CO oxidation and that the reduction of Au^{3+} to Au^0 proceeds below 200 °C. Pretreatment at mild temperatures, *viz*. 200 °C, results in the highest catalytic performance of Au/Al_2O_3 in low-temperature CO oxidation. Alkali (earth) metal oxide additives are most probably structural promoters. The best promoting effect is found for BaO.

KEY WORDS: metallic gold; ionic gold; additives; alkali (earth) metal oxides; promoters; CO oxidation.

1. Introduction

In 1987 striking results showing an exceptionally high activity of gold-based catalysts for low-temperature CO oxidation were published [1]. Compared with highly dispersed supported Pt catalysts, Au-based catalysts can be an order of a magnitude more active [2]. Interestingly, however, large differences in the catalytic activity have been reported in the papers dealing with gold catalysis. For example, Au/Al_2O_3 was reported to be either very inactive [3,4], or as active or even better than Au/TiO_2 [5,6]. Also the effect of various calcination procedures reported in the literature lead to different results. It was reported that for Au/TiO_2 [7,8], Au/Fe_2O_3 [8–10], and Au/MnO_x [11] catalysts, calcination at mild temperatures (100–200 °C) results in more active catalysts than calcination at higher temperatures. There are also reports that uncalcined Au/Al_2O_3 [6] or Au/Y [12] can be very active. In addition, a higher calcination temperature may cause a severe sintering of the gold crystallites [13,14]. On the other hand, it has been reported that a higher calcination temperature may positively influence the catalytic activity of Au/TiO_2 in the sense that a stronger Au–support interaction is created and that this phenomenon leads to a higher catalytic efficiency, even though some sintering of the gold particles was observed [13].

Part of this study deals with the influence of the temperature and the nature of the gas during the pretreatment on the structure and catalytic performance of Au/Al_2O_3. The second part deals with the effect of various alkali (earth) metal oxides and their concentration on the catalytic performance of Au/Al_2O_3 in low-temperature CO oxidation. It was reported that Au supported on $Mg(OH)_2$ or $Be(OH)_2$ displays a high catalytic activity in CO oxidation, especially if the average size of the Au particles is around 2 nm [15]. A beneficial effect of addition of various alkali (earth) metal oxides, such as Li_2O, Rb_2O, MgO and BaO to Au/Al_2O_3 for oxidation of (un)saturated hydrocarbons [16,17], ammonia [18] and reduction of N_2O [19] has also been reported.

* To whom correspondence should be addressed.
E-mail: b.nieuwe@chem.leidenuniv.nl

2. Experimental

2.1. Catalyst preparation

It has been shown in many papers that homogeneous deposition precipitation (HDP) is a suitable method for the preparation of Au-based catalysts [1–4,17,20–22]: the gold deposition onto the support is high, the gold is not buried within the support, and a narrow particle size distribution is obtained.

The unpromoted gold-based catalysts (5 wt% Au) were prepared *via* HDP with urea, using $HAuCl_4 \cdot 3H_2O$ (Aldrich, 99.99%) as the gold precursor. Details concerning the preparation procedures have already been reported [17,20,21]. In the present study the freshly prepared Au/Al_2O_3 catalysts (i.e., after drying) were calcined in pure O_2 at various temperatures (150, 200, 300 and 500 °C) for 2 h. Alternatively, a reductive treatment at various temperatures was also employed.

The mixed supports in the form of MO_x/Al_2O_3 (M: Rb, Li, Ba) were obtained by pore volume impregnation of γ-Al_2O_3 (Engelhard Al-4172P, S_{BET} = 275 m^2 g^{-1}) with a solution of the corresponding nitrates. A detailed description of the experimental procedure is found in [17]. Gold (5 wt%) was deposited onto MO_x/Al_2O_3 (M/Al = 1/15, atomic ratio) by using the same

procedure as for the unpromoted Au/Al_2O_3. For some of the catalysts the preparation procedure was slightly changed. For example, $LiNO_3$ was added to Au/Al_2O_3 *via* pore volume impregnation, followed by drying and calcination in O_2 at 300 °C. The atomic ratio Li/Al was 1/15. This catalyst will be designated as $Li_2O/Au/Al_2O_3$. Furthermore, the influence of the Li_2O loading on the catalytic activity of Au/Al_2O_3 was studied and three $Au/Li_2O/Al_2O_3$ catalysts with different Li/Al ratios, i.e., 1/1, 1/5 and 1/30 have been prepared (all catalysts were 5 wt% Au). These catalysts will be designated as $Au/Li_2O/Al_2O_3\_X$, where $X = 1$, 5 or 30.

2.2. Catalyst characterization

The extent of gold deposition on the support was determined by means of atomic absorption spectroscopy (AAS). The results are summarized in table 1.

BET surface areas of the catalysts were measured by N_2 physisorption at −196 °C using an automatic Qsurf M1 analyzer (Thermo Finnigan). Before each measurement the catalyst was degassed for 2 h in helium at 200 °C in order to remove the adsorbed impurities. For each measurement at least three points have been taken in account to calculate the total surface area of the samples.

XRD measurements for the fresh and spent (i.e., after catalytic test) catalysts were carried out using a Philips Goniometer (PW 1050/25) diffractometer equipped with a PW Cu 2103/00 X-ray tube operated at 50 kV and 40 mA. The average gold particle size was estimated from XRD line broadening by using the Scherrer equation.

HRTEM measurements were performed using a JEOL 2010 microscope with a point-to-point resolution better than 0.2 nm. The sample was mounted on a carbon polymer supported copper micro-grid. A few droplets of a suspension of the ground catalyst in isopropyl alcohol were placed on the grid, followed by drying at ambient conditions. The average gold particles and the particle size distribution were determined by counting at least 300 particles.

DR/UV–Vis spectroscopy experiments have been performed by using a Perkin–Elmer Spectrometer, Lambda 900. The measurements were performed using air-exposed samples between 200 and 850 nm.

TPR measurements were performed by using a lab-scale set-up specially designed for this purpose, with a thermal conductivity detector (TCD) for gas analysis. The gas flow passing through the catalyst bed consisted of 5.5 vol% H_2 in Ar, at a total flow of 25 ml min^{-1}. The reduction degree of gold was estimated by calibration on the basis of the amount of hydrogen needed to completely reduce a known amount of CuO. Prior to each experiment the sample was heated in an Ar flow at 100 °C in order to eliminate the physically adsorbed water. The water produced during the thermal treatment and reduction processes was trapped before the gas mixture reached the TCD, used to monitor the rate of hydrogen consumption.

2.3. Catalytic activity measurements

CO oxidation was carried out in a lab-scale fixed bed reactor in which typically 0.2 g of catalyst was loaded. The standard reactivation procedure consisted of *in-situ* heating the catalyst up to 300 °C for 1 h under H_2 flow. This sequence was applied for Au/Al_2O_3 and $Au/MO_x/Al_2O_3$ (M: Li, Rb and Ba). Alternatively, for Au/Al_2O_3, H_2 was replaced by O_2 or He, in order to study the influence of the reactivation procedure. For that type of measurements the temperature used for reactivation of the catalysts did not exceed the maximum temperature used during first thermal treatment. The feed gases were controlled by mass flow controllers (Bronkhorst) and set to a total flow of 40 ml min^{-1}, which corresponds to a GHSV $\sim$2500 h^{-1}. Diluted CO and O_2 (4 vol%/He) were used to study the oxidation of CO and the reactant ratio was $CO/O_2 = 2/1$. The outlet gas concentration was analysed by a gas chromatograph *(Chrompack CP-2002)* equipped with two columns: a Molsieve 5 Å column for detection of CO and O_2 and a Hayesep A column for CO_2 detection.

Table 1
Catalyst characterization by means of AAS, BET, XRD and HRTEM

Catalyst	Au (wt%)	S_{BET} (m^2 g^{-1})	$d_{Au}{}^a$ (nm)	$S_{Au}{}^a$ (m^2 g^{-1})	$d_{Au}{}^b$ (nm)	$S_{Au}{}^b$ (m^2 g^{-1})	D_{Au} (%)
Al_2O_3	_	275 ± 5	_	_	_	_	_
Au/Al_2O_3	4.1 ± 0.1	260 ± 5	4.3 ± 0.1	2.4 ± 0.1	5.2 ± 0.3	1.5 ± 0.3	11.5 ± 1.1
$Au/Li_2O/Al_2O_3$	4.0 ± 0.3	278 ± 7	3.2 ± 0.1	3.0 ± 0.1	3.0 ± 0.1	2.5 ± 0.1	19 ± 1.0
$Au/Rb_2O/Al_2O_3$	3.5 ± 0.1	294 ± 3	< 3.0	_	2.6 ± 0.3	3.6 ± 0.3	33 ± 1.1
$Au/BaO/Al_2O_3$	3.6 ± 0.2	240 ± 8	< 3.0	_	1.5 ± 0.2	6.2 ± 0.02	55 ± 1.2
$Au/Li_2O/Al_2O_3\_1$	4.5 ± 0.1	261 ± 5	3.0 ± 0.1	3.8 ± 0.1	n.m.	_	_
$Au/Li_2O/Al_2O_3\_5$	4.1 ± 0.2	253 ± 4	4.1 ± 0.2	2.6 ± 0.2	n.m.	_	_
$Au/Li_2O/Al_2O_3\_30$	4.2 ± 0.1	269 ± 7	< 3.0	_	n.m.	_	_
$Li_2O/Au/Al_2O_3$	4.1 ± 0.1	270 ± 9	3.8 ± 0.1	2.8 ± 0.1	n.m.	_	_

$d_{Au}{}^a$: mean diameter of gold particles, XRD, fresh catalysts (nm); $d_{Au}{}^b$: mean diameter of gold particles, HRTEM, fresh catalysts (nm); $S_{Au}{}^a$: gold surface area, XRD (m^2 g^{-1}); $S_{Au}{}^b$: gold surface area, HRTEM (m^2 g^{-1}); D_{Au}: gold dispersion, HRTEM; n.m.: not measured.

The reactant mixture was stabilized for at least 30 min at room temperature. Afterwards at least two consecutive heating–cooling reaction cycles were performed. To compare the catalytic performance, the results of the second heating cycle are considered. Third and additional heating–cooling cycles gave almost similar results as those of the 2nd cycle. The specific reaction rate, r, expressed as the number of CO (moles) transformed over the amount of Au (moles) per second was also determined.

After performing the test reaction, the catalysts were again analysed by XRD.

3. Results

3.1. Catalyst characterization

3.1.1. AAS, BET, XRD and HRTEM results

A summary of all the characterization results obtained by using AAS, BET, XRD and HRTEM is presented in table 1. In addition, where possible, the metallic surface area of gold was estimated based on the XRD or HRTEM results. The HRTEM results have been also used to estimate the Au dispersion.

A comparison of the XRD results obtained for Au/Al_2O_3 catalysts in two different states (calcined at 300 °C in an oxygen flow or dried at 80 °C), support-only (Al_2O_3) and Au-sponge are depicted in figure 1. The XRD pattern of Au-sponge shows the typical diffraction pattern of metallic Au, i.e., the presence of two diffraction lines at $2\theta = 38.2°$ ($d = 2.35$ Å) and $2\theta = 43.4°$ ($d = 2.03$ Å). As expected, dried-Au/Al_2O_3 does not show any diffraction pattern characteristic of metallic gold, it only resembles the structure of γ-Al_2O_3. On the other hand, calcined-Au/Al_2O_3 shows mainly the diffraction lines of $2\theta = 38.2°$, which is, however, relatively broad, typical of relatively small crystallites. The average size of the gold particles as calculated by using the main diffraction line of $2\theta = 38.2°$ is around 4.3 nm. A much smaller diffraction line is visible at $2\theta = 43.4°$.

Figure 2 shows the influence of the gas phase composition (H_2 or O_2) and temperature of the pretreatment (150, 300 and 500 °C) on the structure of Au/Al_2O_3 as determined by XRD. A pretreatment in either O_2 or H_2 at 150 °C is able to generate metallic gold (diffraction line at $2\theta = 38.2°$). The Au crystallite size is around 3 nm. In addition, no significant difference was found in the size of the gold particles for a pretreatment in H_2 and O_2. By increasing the temperature, the average size of the Au particles increases slightly (a treatment at 300° in O_2 forms gold particles of 4.3 nm). In an atmosphere of hydrogen a further increase in treatment temperature (500 °C) causes a minor increase in the particle size from 4.3 to 4.8 nm, whereas no change was observed for heating in O_2 (4.3 nm). However, the difference caused by using H_2 or O_2 is not large, even at 500 °C large agglomeration of the gold crystallites was not found.

If very small gold crystallites or amorphous phases were present (Au/BaO/Al_2O_3, Au/Rb_2O/Al_2O_3 and Au/Li_2O/Al_2O_3_30), XRD was not able to detect the gold signal. By comparing the values of d_{Au}[a] (table 1) it is clear that the presence of the alkali (earth) metal oxides has a beneficial effect on the stabilization of the small Au crystallites during preparation and further thermal treatments.

The metallic surface area (XRD results)—table 1, was calculated by assuming that the gold particles are hemispherical in shape with the flat side on the support, according to the following formula:

$$S_{Au} = 50000 \cdot W/\rho \cdot d \quad (1)$$

where W corresponds to the gold loading, ρ is the density of gold (19.3 $cm^3\ g^{-1}$) and d is the diameter of gold particles as determined by XRD (Å). According to the results presented in table 1, S_{Au} varies between 2.4 $m^2\ g^{-1}$ (Au/Al_2O_3) and 3.8 $m^2\ g^{-1}$ (Au/Li_2O/Al_2O_3_1).

A typical HRTEM image of the gold particles of Au/Al_2O_3 catalyst is shown in figure 3. The gold particles (black dots in figure 3) are fairly homogeneously

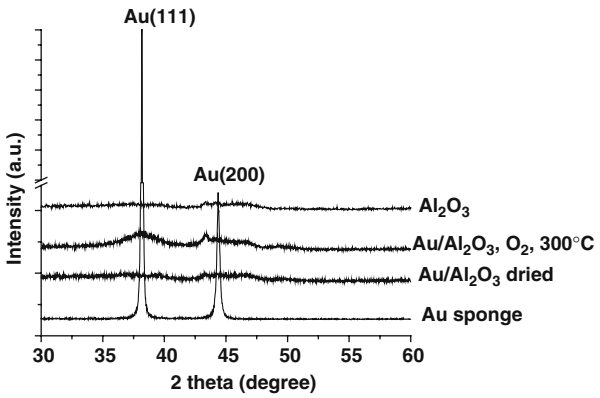

Figure 1. Comparison of XRD patterns of calcined-Au/Al_2O_3 (300 °C, O_2), dried-Au/Al_2O_3, Au-sponge and Al_2O_3 support.

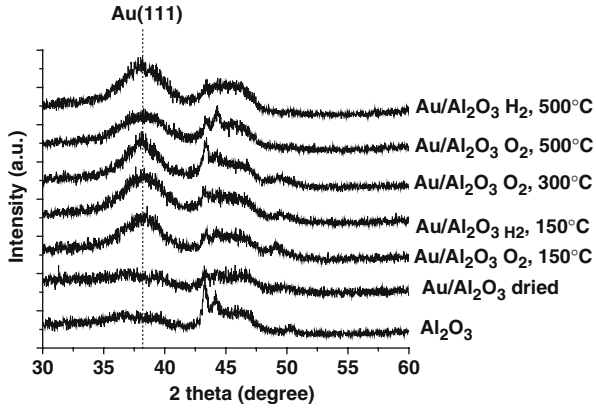

Figure 2. The influence of the pretreatment (gas and temperature) on the structure of Au/Al_2O_3 catalysts (XRD measurements).

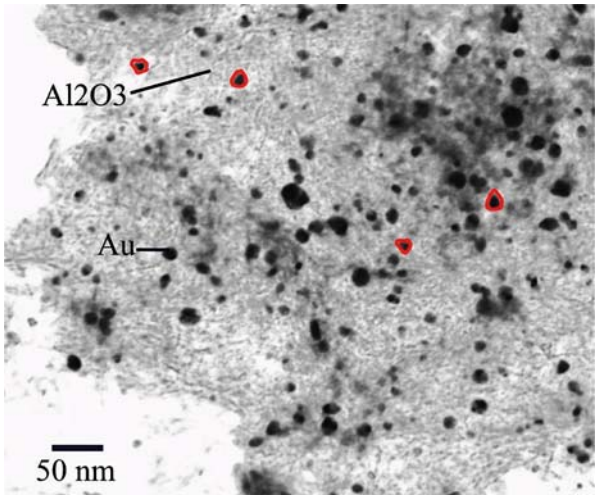

Figure 3. HRTEM image of Au/Al_2O_3.

distributed over the alumina support (grey regions). On average, the gold particles were rather large (5.2 nm). In addition, it is also visible in figure 3 that some of the gold particles do not exhibit a round shape, but rather a truncated one.

The Au particle size distribution (HRTEM) of Au/Al_2O_3, $Au/Rb_2O/Al_2O_3$ and $Au/BaO/Al_2O_3$ is presented in figure 4. There is a significant difference concerning the particle size distribution of the samples with or without additive. The growth of the large gold particles at the expense of the smaller Au crystallites found for Au/Al_2O_3 is prevented in the presence of alkali (earth) metal oxides.

The metallic surface area (HRTEM) varies between 1.5 $m^2\ g^{-1}$ (Au/Al_2O_3) and 6.2 $m^2\ g^{-1}$ ($Au/BaO/Al_2O_3$). The differences between the values of the gold surface area determined by HRTEM and XRD may be related to the experimental limitations of each technique. However, it should be emphasized that both techniques are not completely suitable for this type of determinations and that the results may be considered only as a relative measure of the metallic surface area of the catalysts. A dispersion of 55% was calculated for $Au/BaO/Al_2O_3$, which considerably exceeds the estimated dispersion of Au/Al_2O_3 (11.5%).

3.1.2. DR/UV–Vis results

Metal nanoparticles have optical properties that are absent in the bulk material as well as for the individual atoms. These optical properties are determined by both their size and shape [23]. Fine gold particles, in the nanometer range, exhibit a surface plasmon peak centred between 500 and 600 nm. The relation between the mean particle diameter, the shape of the particles and the peak position is also influenced by the dielectric function of the supporting or surrounding medium, as well as by possible particle interactions deviating from the single-particle assumption of Mie's theory [24].

Although it is generally accepted that the peak position of Au in the metallic state is between 500 and 600 nm, the peak positions of the ionic gold species are still under discussion. However, it was reported that Au^+ cations display an absorption band around 240 nm, whereas small clusters such as $(Au)_n^{\delta+}$ exhibit a band around 390 nm [25].

Figure 5 presents the optical spectra of Au/Al_2O_3 calcined at 300 °C in O_2, dry-Au/Al_2O_3, Au-sponge and Al_2O_3. As expected, dry-Au/Al_2O_3 does not exhibit the plasmonic oscillation mode of nanosized gold particles, since no metallic gold is present in the sample. The optical spectra of dry-Au/Al_2O_3 show a small shoulder around 260 nm. This peak corresponds to the one reported in literature for Au^+ [25]. On the other hand, the optical spectrum of prereduced Au-sponge also shows a shoulder in that region, although a little shifted to lower wavelength (240 nm) and less intense than for

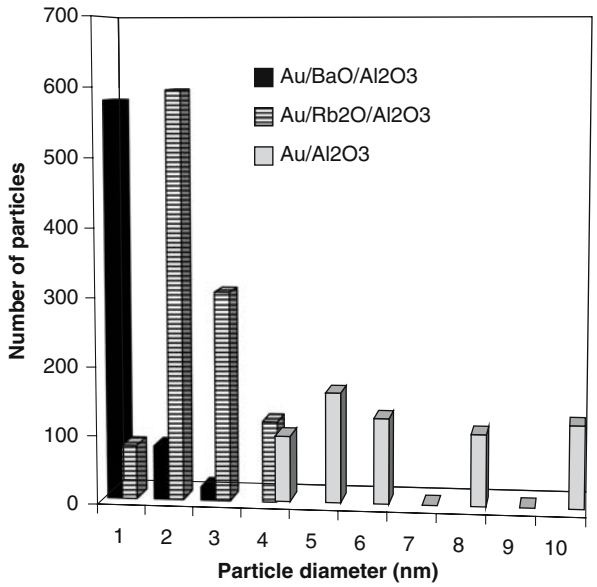

Figure 4. Particle size distribution as determined by HRTEM for Au/Al_2O_3, $Au/Rb_2O/Al_2O_3$ and $Au/BaO/Al_2O_3$.

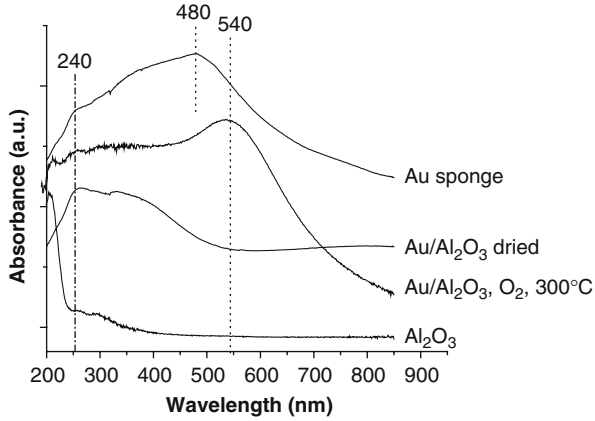

Figure 5. DR/UV–Vis spectra of calcined-Au/Al_2O_3, dried-Au/Al_2O_3, Au-sponge and Al_2O_3 support.

dry-Au/Al_2O_3. Thus, the assignment of the peak at 260 nm to Au^+ is open to doubt, since prereduced Au-sponge contains only Au^0. The calcined-Au/Al_2O_3 displays very clearly the plasmon band characteristic of metallic gold.

The same peak but with different shape and shifted to lower wavelength (480 nm) is observed for Au-sponge. As was mentioned before, the shape of the peak, defined here as the full-width-at-half-maximum (FWHM) of the peak, strongly depends on the shape and the size of the gold particles. Thus, the relatively large shift, from 540 to 480 nm, accompanied by the variation of FWHM may be explained in terms of the huge difference in the size of the gold particles of the two samples: an average size of 74 nm for sponge-Au, and 4.3 nm for calcined-Au/Al_2O_3. A decrease in the size of the gold particles causes a red shift in the absorption peak, accompanied by a larger FWHM in the "intrinsic size region" (mean diameter smaller than 25 nm) [23]. For large particles the opposite effect was reported; the FWHM increases with increasing size, in the "extrinsic size region" (mean diameter larger than 25 nm). Thus, the apparent differences in optical spectra of calcined-Au/Al_2O_3 and Au-sponge can be explained on the basis of the size effect. In addition, the shape of the gold particles may differ significantly for the two samples, resulting in an additional optical difference.

DR/UV–Vis spectroscopy was also used to characterize the Au/Al_2O_3 catalyst subjected to various thermal treatments, under oxygen or hydrogen flow. Figure 6a presents the spectra of Au/Al_2O_3 catalyst heated in O_2 at various temperatures (150, 200, 300 and 500 °C) and figure 6b shows the corresponding spectra of Au/Al_2O_3 treated in H_2 at 150, 200 and 300 °C.

The typical plasmon band of Au nanocrystallites appears already after a heat-treatment at 150° and no effect of the nature of the gas was found on the formation of Au^0. However, it should be noted that the extent of reduction cannot be quantified by these measurements. The small peak at 260 nm (dry-Au/Al_2O_3) decreases upon heating and, eventually, is weaker if H_2 is used. Although the evolution of this peak changes with the temperature, we still cannot conclude that this peak belongs to Au^+, since reduced Au-sponge reveals a similar feature in that region of the spectra.

The variation of the plasmon band of small gold particles for the bicomponent gold-based catalysts with alkali (earth) metal oxide additives is presented in figure 7. For comparison, the DR/UV–Vis spectra of the supports are also included. The support signal was not subtracted, in order to avoid the appearance of false peaks. The plasmon band of Au^0 is visible for all the samples. Notice the very broad bands for $Au/Rb_2O/Al_2O_3$ and $Au/BaO/Al_2O_3$ and a slight shift of the peak maximum due to the size effect. Different concentrations of Li_2O did not produce any additional features in the optical behaviour of Au-based catalysts, compared with the DR/UV–Vis spectrum of $Au/Li_2O/Al_2O_3$.

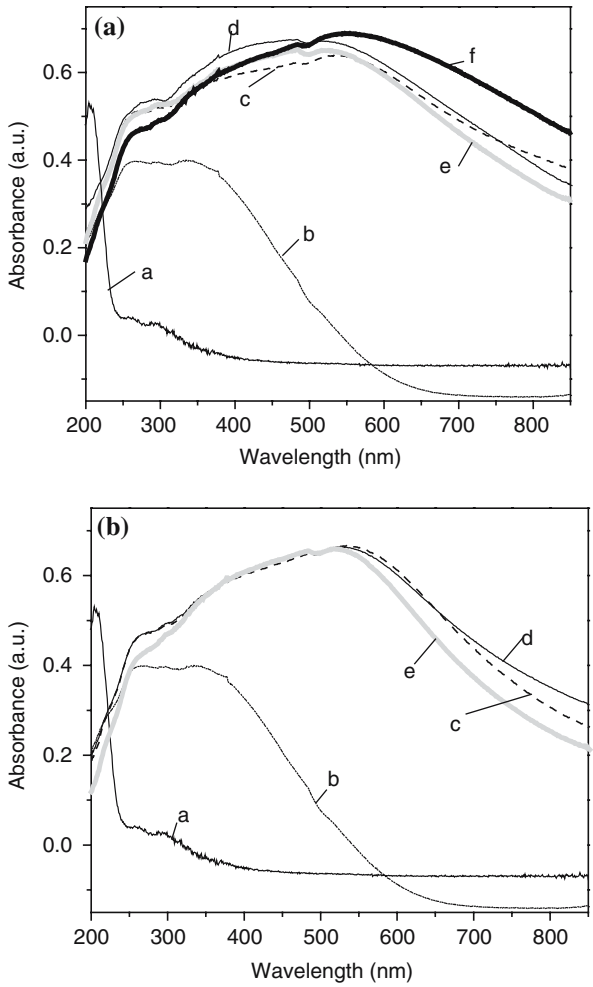

Figure 6. DR/UV–Vis spectra of samples pretreated in O_2 (a) and H_2 (b). Al_2O_3 (a), dried-Au/Al_2O_3 (b), Au/Al_2O_3 150 °C (c), Au/Al_2O_3 200 °C (d), Au/Al_2O_3 300 °C (e), Au/Al_2O_3 500 °C (f).

3.1.3. TPR results

TPR spectroscopy was used to study in more detail the reduction of unpromoted Au/Al_2O_3 in the presence of hydrogen. This technique has not been used often for gold-based catalysts and, interestingly, the few papers dealing with this subject report a rather broad range of the reduction temperature of alumina-supported gold catalysts. For example, for Au/Al_2O_3 it was reported that reduction of Au proceeds in three steps: first at −93 °C Au^sO_x is being reduced, then at 27 °C the reduction of Au^sCl_y takes place, while upon further increasing the temperature, at 727 °C the reduction occurs of gold ions (Au^I) incorporated in the subsurface of alumina support [26]. Another paper reported that the reduction of Au in Au/MgO takes place during a single process with a maximum at 142 °C, whilst if Fe or Mn are added to Au/MgO, the reduction temperature of Au increases slightly to 156 and 170 °C, respectively [27]. No information was provided about the reduction of the Fe and Mn oxide additives. If gold was present as $Au(CH_3)_2$(acac) (acac: acetylacetonate), the reduction of

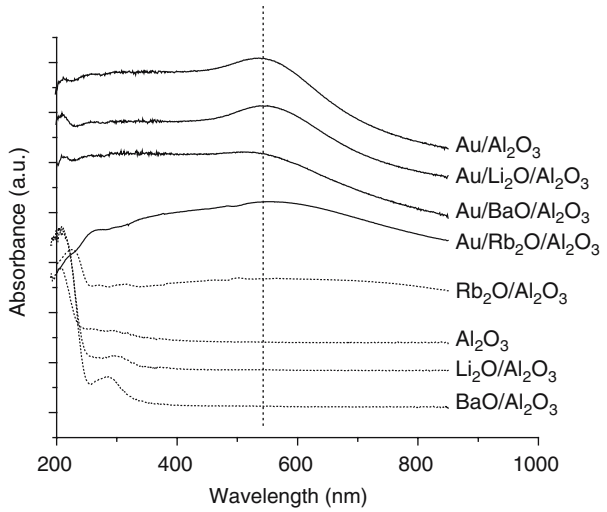

Figure 7. DR/UV–Vis optical spectra of different gold-based catalysts and the corresponding supports.

Au particles was found at around 148 °C, while if gold was present as supported mononuclear Au, the reduction temperature increased to 208 °C [28]. Although very different temperatures were reported for gold reduction, all these papers agree that gold was present initially as Au^{3+}. Other papers address the influence of gold addition on the reducibility of CeO_2, FeO_x or Co_3O_4, without discussion concerning gold reduction [29,30]. It should be noted that different results may be partly caused by experimental differences, such as in heating ramp, flow rate or the concentration of the reducing gas.

The reduction profile of Au_2O_3 (Aldrich) is depicted in figure 8a, while figure 8b shows a comparison between the TPR spectra of Au_2O_3/Al_2O_3 and Au/Al_2O_3.

The reduction of Au_2O_3, proceeds at 86 °C and corresponds to the reduction of Au^{3+} to Au^0. The small shoulder at 137 °C is due to the reduction of Au^+ to Au^0, which is, however, much smaller than the main peak at 86 °C. When gold is deposited on alumina, *viz*. Au_2O_3/Al_2O_3, the reduction profile looks quite different (figure 8b). The reduction of Au^{3+} to Au^0 proceeds in one single step and is shifted to higher temperature (163 °C). The calculated amount of Au^{3+}, which is reduced to Au^0 corresponds to 3.65 wt% Au, in line with the AAS results. This reduction temperature is in agreement with results reported in [27]. The difference in the reduction profiles of Au_2O_3 and Au_2O_3/Al_2O_3 may be explained upon considering that in the former case the size of the gold oxide particles is much larger than in the latter case. For this reason, during the first reduction step of Au_2O_3, partly reduced Au grains are formed, which probably encapsulate small ionic gold grains. These will be further reduced to metallic gold in the next reduction step. When gold is deposited on alumina, the gold concentration is much lower than in the case of Au_2O_3 and, consequently, the gold particles are more accessible to hydrogen from the gas phase. In addition, the interaction formed during the preparation step between Au and the support shifts the reduction temperature of the gold species to higher temperature, compared to unsupported Au_2O_3. In addition, a large difference in the hydrogen consumption is observed upon comparison of the intensity peaks of Au_2O_3 and Au_2O_3/Al_2O_3. The negative peak observed at higher temperature for Au_2O_3/Al_2O_3 might be due to some desorption process, since this sample was not subjected to precalcination. The "hydrogen consumption" of Au/Al_2O_3 is much lower than that of Au_2O_3/Al_2O_3 and based on the TPR profile of Au_2O_3/Al_2O_3, all the gold is in its reduced state at 300 °C.

3.2. Catalytic activity measurements

3.2.1. Unpromoted Au/Al_2O_3

Figure 9a shows the catalytic behaviour of Au/Al_2O_3 that was subjected to calcination (i.e., the usual procedure) at different temperatures (150, 200, 300 or 500 °C). A second thermal treatment of the catalysts, carried out *in-situ*, was performed at the same temperature as used during the first treatment. Clearly, all the

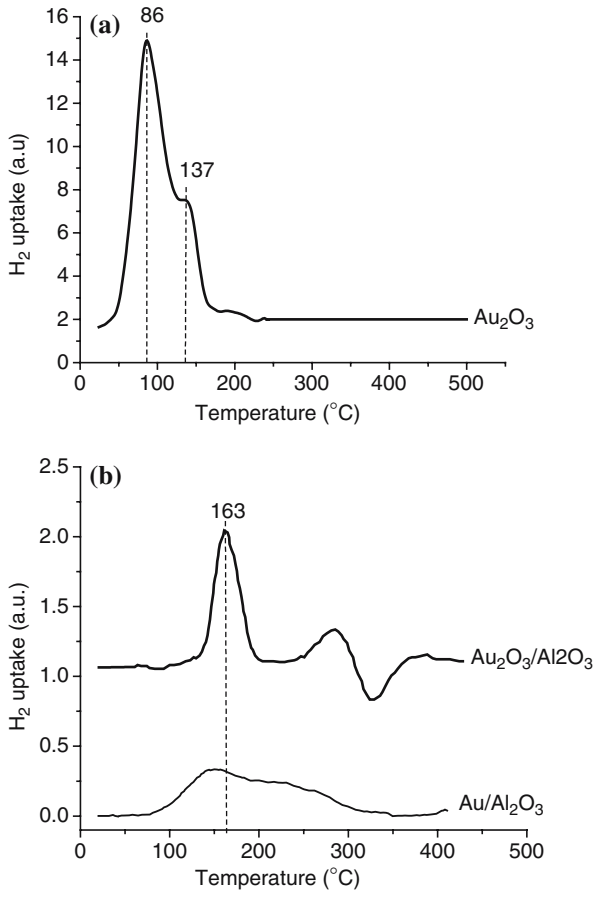

Figure 8. TPR reduction profile of Au_2O_3 (a) and Au_2O_3/Al_2O_3 and Au/Al_2O_3 (b). The reducing gas consisted of 5.5 vol% H_2 in Ar, at a total flow of 25 ml min^{-1}.

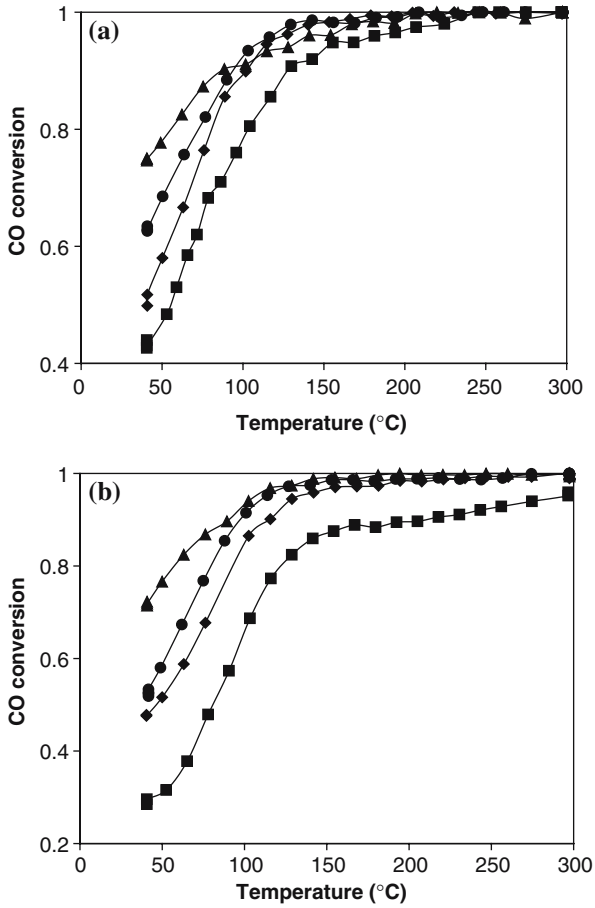

Figure 9. CO conversion versus temperature over calcined (a) and reduced (b) Au/Al_2O_3. The symbol in (a) corresponds to: 200/no pretreatment (▲), 300/H_2/300 (●), 500/H_2/300 (♦), 150/He/150 (■). The symbols in (b) correspond to 200/He/200 (▲), 300/He/300 (●), 500/He/300 (♦), 150/He/150 (■). Reactant ratio: CO:O_2 = 2:1.

catalysts are highly active in CO oxidation and at around 140 °C complete CO conversion is obtained. However, the thermal treatment influences the catalytic performance of Au/Al_2O_3. Calcination at 200 °C without any additional treatment results in the highest activity. Less active catalysts are obtained following calcination at 500 °C (due to some sintering), or at 150 °C (most likely due to incomplete reduction of Au^{3+} to Au^0). This assumption is supported by the TPR results presented above. However, it should be mentioned that after calcination at 150 °C the colour of the catalyst was changed from yellow to purple, indicating decomposition of oxidic gold to Au^0. Full reduction probably needs higher temperatures. It should be mentioned that conversion of CO over bare alumina is not significant up to 300 °C.

A similar trend in the catalytic performance of Au/Al_2O_3 is obtained if O_2 is replaced by H_2. The results are presented in figure 9b. The most active sample is obtained after H_2 treatment at 200 °C.

All the data concerning the catalytic performance of Au/Al_2O_3 catalysts are presented in table 2. The data include the temperature required for 95% CO conversion, the CO conversion at 70 °C (X_{70}), the specific reaction rate r calculated at 70 °C and the average gold particle size after ($d_{Au}{}^b$) reaction (XRD).

The specific reaction rate r shows the largest value for the calcined Au/Al_2O_3 without any *in-situ* post-treatment. There is a difference between the values of r for the samples treated at 150° in O_2 or H_2: the former being more active. Possibly, at 150 °C, contaminants are easier removed in O_2. These differences are not due to a particle size effect since the average size of the gold particles is nearly the same for all samples except for treatment at 500 °C. Thus, the differences observed in the catalytic performance are most probably due to the chemical state of gold, which depends on the thermal treatment. However, as a secondary effect, the particle size effect will play a role as well.

3.2.2. *Alkali (earth) metal oxides as additives*

Figure 10a shows the conversion of CO versus temperature over alkali (earth) metal oxide-promoted Au/Al_2O_3 (second heating) and Li_2O/Al_2O_3 support. The influence of the Li_2O concentration on the catalytic performance of Au/Al_2O_3 is presented in figure 10b.

Table 2
$T_{95\%}$, the conversion at 70 °C (X_{70}), the specific reaction rate, r, the average size of the gold particles for the spent ($d_{Au}{}^b$) Au/Al_2O_3 (XRD)

Treatment	$d_{Au}{}^b$ (nm)	$T_{95\%}$ (°C)	X_{70}	$r \times 10^3$ (mol CO mol^{-1} Au s^{-1})
O_2/150/He	3.0 ± 0.1	168	0.61	5.5 ± 0.1
O_2/200/He	3.0 ± 0.3	117	0.81	6.3 ± 0.1
O_2/200/no treatment	3.0 ± 0.2	135	0.85	6.7 ± 0.1
O_2/200/H_2	3.0 ± 0.2	128	0.79	6.2 ± 0.2
O_2/300/H_2	*3.0 ± 0.2*	*112*	*0.78*	*5.5 ± 0.1*
O_2/300/no treatment	3.0 ± 0.1	162	0.79	5.5 ± 0.1
O_2/500/H_2	4.5 ± 0.4	114	0.71	5.4 ± 0.1
H_2/150/He	3.3 ± 0.3	290	0.41	3.3 ± 0.1
H_2/200/He	< 3.0	107	0.84	6.6 ± 0.1
H_2/200/H_2	< 3.0	84	0.95	6.4 ± 0.1
H_2/300/He	3.4 ± 0.1	113	0.74	5.3 ± 0.1
H_2/500/He	4.6 ± 0.2	133	0.63	5.4 ± 0.1

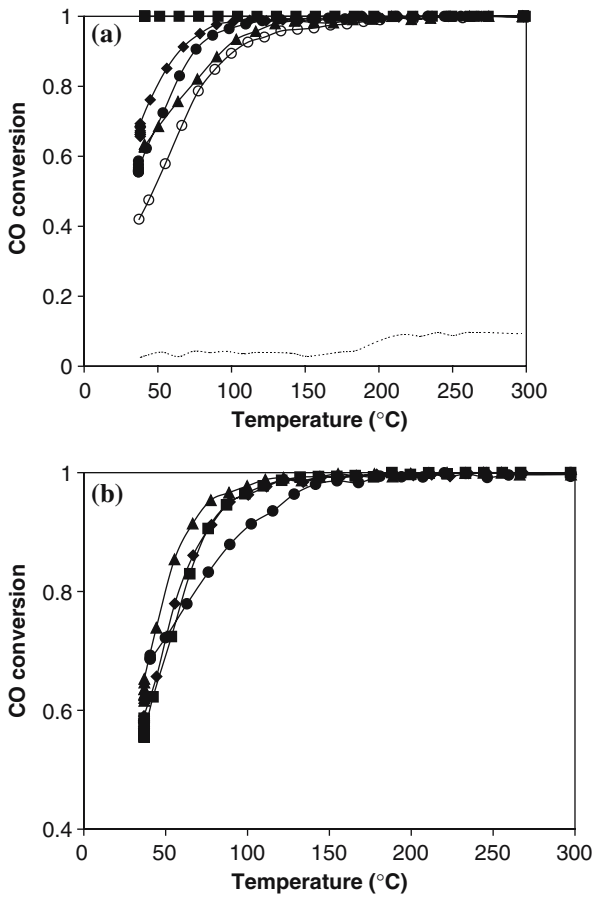

Figure 10. CO conversion versus temperature over Au/BaO/Al_2O_3 (■), Au/Rb_2O/Al_2O_3 (♦), Au/Li_2O/Al_2O_3 (●), Au/Al_2O_3 (O_2/300/H_2) (▲), Li_2O/Au/Al_2O_3 (○), Li_2O/Al_2O_3 (–) (a); Au/Li_2O/Al_2O_3_30 (▲), Au/Li_2O/Al_2O_3_5 (♦), Au/Li_2O/Al_2O_3_15 (■), Au/Li_2O/Al_2O_3_1 (●) (b).

The best performance is obtained for Au combined with BaO and full CO conversion is reached at room temperature. The catalytic activity of Au/Al_2O_3 is also enhanced in the presence of Rb_2O and Li_2O. The addition of Li_2O after Au deposition onto the support produces a decrease in the catalytic performance compared with the other alkali (earth)-promoted Au/Al_2O_3 catalysts. Concerning the effect of Li_2O, the order of addition significantly influences the catalytic performance (see table 3). Most likely, the interaction between Au and the support, crucial for high catalytic activity, is stronger if Li_2O is first added to alumina.

The loading of Li_2O influences both the size of the Au particles and the catalytic performance of Au/Al_2O_3 (see table 3). The best result is obtained for an atomic ratio Li:Al = 1:30 (1 wt% Li_2O). A larger amount of Li_2O (atomic ratio Li:Al = 1:1) causes only a small increase in the catalytic performance. In fact, the catalyst with the highest Li_2O concentration shows a lower r compared with the unpromoted Au/Al_2O_3. A summary of all the data concerning the promoting effect of various alkali (earth) metal oxides on the catalytic performance of Au/Al_2O_3 is presented in table 3.

In spite of its slightly lower r-value Au/BaO/Al_2O_3 shows the lowest $T_{95\%}$. Au sintering was not observed using XRD.

4. General discussion

4.1. Catalyst activation-pretreatment

Concerning the influence of the thermal treatment and the nature of the employed gas (O_2, H_2, or He) on the catalytic performance of Au/Al_2O_3, it was found that the best results are obtained if the as-prepared (i.e., dried) catalyst is subjected to an O_2 treatment at 200 °C. After a treatment in H_2 or O_2 at 200 °C, presumably all the gold is transformed into Au^0 (TPR results support this model). A subsequent thermal treatment does not significantly influence the catalytic performance. The fact that "no pretreatment" proved to be a better choice than any other possible treatment may be connected to the presence of some adsorbed water on the surface of the catalyst. However, this is unlikely since the results shown correspond to the second heating cycle, and, presumably, the amount of adsorbed water after one heating–cooling cycle is relatively small. Regarding the overall effect of the thermal treatment of the dried samples, the variation of the catalytic activity correlates to some extent with the average size of the Au particles, although not completely. Clearly, the variation of the average particle size of the various catalysts used in the

Table 3
$T_{95\%}$, the conversion at 70 °C (X_{70}), the specific reaction rate, r, the average size of the gold particles for the spent ($d_{Au}{}^b$) Au-based catalysts (XRD)

Catalyst	$d_{Au}{}^b$ (nm)	$T_{95\%}$ (°C)	X_{70}	$r \times 10^3$(mol CO mol^{-1} Au s^{-1})
Au/Li_2O/Al_2O_3_15	3.2 ± 0.1	89	0.87	6.9 ± 0.1
Au/Li_2O/Al_2O_3_30	3.0 ± 0.1	77	0.93	7.4 ± 0.1
Au/Li_2O/Al_2O_3_5	4.7 ± 0.3	90	0.88	7.2 ± 0.2
Au/Li_2O/Al_2O_3_1	3.1 ± 0.3	123	0.8	4.9 ± 0.1
Li_2O/Au/Al_2O_3_15	3.6 ± 0.2	127	0.71	5.9 ± 0.1
Au/Rb_2O/Al_2O_3	< 3.0	78	0.92	8.9 ± 0.1
Au/BaO/Al_2O_3	< 3.0	< 25	1	7.6 ± 0.1[a]

[a]This value corresponds to 100% CO conversion.

present study is too small for definite conclusion. Even a treatment at 500 °C did not produce a severe sintering of the gold particles.

Based on the above presented results, it is concluded that the metallic gold is the major active species for CO oxidation. For unpromoted Au/Al_2O_3 a thermal treatment at 200 °C is the optimum temperature for the high activity. A similar result was reported for Au/TiO_2 and Au/Co_3O_4 [6].

4.2. The effect of MO_x on the catalytic activity of Au/Al_2O_3. The active sites

The results presented throughout this paper show that the catalytic performance of Au/Al_2O_3 is improved by using alkali (earth) metal oxides as additives. Most probably the beneficial effect of the additives can be attributed to a change of the morphology and size of the Au particles due to the addition of alkali (earth) metal oxides to Al_2O_3.

The detailed study concerning the promoter effect of Li_2O revealed that the catalytic performance of Au-based catalysts is influenced by both the concentration of Li_2O and the order of its addition to Au/Al_2O_3. Although there is a clear effect of the additives on the size of the gold particles, which, in turn, influences the Au surface area (i.e., active sites), a direct correlation between the size and the catalytic activity could not be established. For example $Au/Li_2O/Al_2O_3$_1 shows the largest metallic surface area, according to the HRTEM results, but the catalytic activity in CO oxidation is not the highest one.

The role of the alkali (earth) metal oxides on the activity of Au/Al_2O_3 is not clear yet, although this topic has attracted a lot of research interest in the past years. It was suggested that their role would be mostly directed towards stabilization of the Au nanoparticles [14,19,31]. In our opinion the high activity of gold nanoparticles is connected with a relatively high abundance of low-coordinated Au atoms that may be responsible for the high activity [32–34]. Based on theoretical studies it has been suggested that in the case of Au/Mg(100), the role of MgO is two-fold. First it may provide excess electrons to the Au clusters, forming ionic bonds to the peroxo part of the proposed $CO \cdot O_2$ reaction intermediate [34–36]. Second, the authors suggested that the interface boundary Au–MgO is most important for high activity. An earlier study showed that the presence of some alkali (Li, Na, K) metal oxides is beneficial for the catalytic activity of Au/MnO_x and it was hypothesized that this promotion might be connected with the suppression of CO_2 retention [37]. Using FTIR it was found that when MO_x (M: Mg, Mn and Fe) is added to Au/Al_2O_3, both the C–O stretching frequency and the CO adsorption capacity are significantly affected (decreased) [14]. MgO induced the smallest effect on the adsorption capacity of Au/Al_2O_3, compared with MnO_x and FeO_x. Thus, FTIR showed that the nature of MO_x influences the adsorption of CO.

On the other hand, Au-based catalysts either deposited on non-reducible metal oxides such as Al_2O_3 or MgO, or doped with alkali (earth) metal oxides showed high activity in low-temperature CO oxidation. This could be due to lowering of the reaction barrier of O_2 adsorption by these additives. It is widely accepted that O_2 activation during CO oxidation is the most difficult step and the inertness of gold bulk surfaces is understood from the poor affinity toward molecular oxygen [38–41]. It was also suggested that the support material induces strain in the gold particles due to the mismatch of the lattice at the interface, an effect that is more pronounced in small gold particles than in larger ones [42].

It is generally accepted that CO adsorption takes place on Au [43,44] and at the Au–support interface [45,46]. Moreover, based on DFT calculations, it was reported that the availability of many low-coordinated Au atoms, with an increased number of steps and kinks, accommodated by the defects of the support, is most important to obtain an active Au-based catalyst [32,33,42].

Taking into account these models, the main issue remains the activation of oxygen. Recently, DFT calculations showed that O_2 can adsorb at the Au–support interface, but the dissociation of O_2 cannot occur at low temperatures [47]. It was proposed that the reaction occurs on Au steps *via* a two-step mechanism involving reaction between CO adsorbed on Au defects and O_2 accommodated at the Au–support interface [47].

It is suggested, based on all relevant data reported and on the results presented in this study, that CO is adsorbed on Au and at the Au–support interface and reacts with the oxygen, most probably at the interface. It has been proven that the alkali (earth) metal oxides additives act as structural promoters [16,17] and possibly also help in O_2 activation.

5. Conclusions

Various characterization techniques indicate that the reduction of Au^{3+} to Au^0 takes place below 200 °C and that the working state of Au is metallic. The (alkali) earth metal oxides inhibit the growth of the very small Au particles during preparation and catalytic reaction. Unpromoted Au/Al_2O_3 catalysts are highly active in low-temperature CO oxidation. It is found that a thermal treatment at 200 °C in oxygen applied on the as-prepared (dried) samples is more efficient than a thermal treatment at 150, 300 or 500 °C.

Important promoting effects are obtained by using additives of the type of alkali (earth) metal oxides. The catalytic activity of Au/Al_2O_3 is dramatically improved upon addition of BaO and full conversion of CO is already obtained at room temperature.

Acknowledgments

The Netherlands Organization for Scientific research, NWO (Grant NWO/CW 99037 and NWO #047.015.003) is gratefully acknowledged for financial support.

References

[1] M. Haruta, T. Kobayashi and N. Yamada, Chem. Lett. 2 (1987) 405.
[2] M. Haruta, Stud. Surf. Sci. Catal. 110 (1997) 123.
[3] M.M. Schubert, V. Plzak, J. Garche and R.J. Behm, Catal. Lett. 76 (2001) 143.
[4] M. Okumura, S. Nakamura, S. Tsubota, T. Nakamura, M. Azuma and M. Haruta, Catal. Lett. 51 (1998) 53.
[5] C.K. Costello, M.C. Kung, S.-O. Oh, Y. Wang and H.H. Kung, Appl. Catal. A 232 (2002) 159.
[6] A. Wolf and F. Schuth, Appl. Catal. A 226 (2002) 1.
[7] F. Boccuzzi, A. Chiorino, M. Manzoli, P. Lu, T. Akita, S. Ichikawa and M. Haruta, J. Catal. 202 (2001) 256.
[8] E.D. Park and J.S. Lee, J. Catal. 186 (1999) 1.
[9] N.A. Hodge, C.J. Kiely, R. Whyman, M.R.H. Siddiqui, G.J. Hutchings, Q.A. Pankhurst, F.E. Wagner, R.R. Rajaram and S.E. Golunski, Catal. Today 72 (2002) 133.
[10] S. Minico, S. Scire, C. Crisafulli and Galvagno, Appl. Catal. B 34 (2001) 277.
[11] S.-J. Lee, A. Gavriilidis, Q.A. Pankhurst, A. Kyek, F.E. Wagner, P.C.L. Wong and K.L. Yeung, J. Catal. 200 (2001) 298.
[12] J.-N. Lin, J.-H. Chen, C.-Y. Hsiao, Y.-M. Kang and B.-Z. Wan, Appl. Catal. B 36 (2002) 19.
[13] S. Tsubota, T. Nakamura, K. Tanaka and M. Haruta, Catal. Lett. 56 (1998) 131.
[14] R.J.H. Grisel, *Supported Gold Catalysts for Environmental Applications*, PhD Thesis, Leiden University (2002).
[15] S. Tsubota, M. Haruta, T. Kobayashi, A. Ueda and Y. Nakahara, in: *Preparation of Catalysts V* (Elsevier, 1991), p. 695.
[16] A.C. Gluhoi, B.E. Nieuwenhuys, Catal. Today (2005) submitted.
[17] A.C. Gluhoi, N. Bogdanchikova and B.E. Nieuwenhuys, J. Catal. 232 (2005) 96.
[18] S.D. Lin, A.C. Gluhoi and B.E. Nieuwenhuys, Catal. Today 90 (2004) 3.
[19] A.C. Gluhoi, M.A.P. Dekkers and B.E. Nieuwenhuys, J. Catal. 219 (2003) 197.
[20] R.J.H. Grisel, P.J. Kooyman and B.E. Nieuwenhuys, J. Catal. 191 (2000) 430.
[21] A.C. Gluhoi, N. Bogdanchikova and B.E. Nieuwenhuys, J. Catal. 229 (2005) 154.
[22] G.C. Bond and D.T. Thompson, Catal. Rev. Sci. Eng. 41 (1999) 319.
[23] S. Link and M.A. El-Sayed, J. Phys. Chem. B 103 (1999) 4212 and refs. therein .
[24] P. Claus, A. Bruckner, C. Mohr and H. Hofmeister, J. Am. Chem. Soc. 122 (2000) 11430 and refs. therein.
[25] J.L. Margitfalvi, A. Fasi, M. Hegedus, F. Lonyi, S. Gobolos and N. Bogdanchikova, Catal. Today 72 (2002) 157 and ref. therein.
[26] C.-K. Chang, Y.-J. Chen and C.-T. Yeh, Appl. Catal. A 174 (1998) 13.
[27] J.L. Margitfalvi, M. Hegedus, A. Szegedi and I. Sajo, Appl. Catal. A 272 (2004) 87.
[28] J. Guzman and B.C. Gates, J. Phys. Chem. B 107 (2003) 2242 and refs. therein.
[29] D. Andreeva, Gold Bull. 35 (2002) 82.
[30] S. Scire, S. Minico, C. Crisafulli, C. Satriano and A. Pistone, Appl. Catal. B 40 (2003) 43.
[31] A.C. Gluhoi, S.D. Lin and B.E. Nieuwenhuys, Catal. Today 90 (2004) 175.
[32] N. Lopez, J.K. Norskov, T.V.W. Janssens, A. Carlsson, A. Puig-Molina, B.S. Clausen and J.D. Grunwaldt, J. Catal. 225 (2004) 86.
[33] N. Lopez, T.V.W. Janssens, B.S. Clausen, Y. Xu, M. Mavrikakis, T. Bligaard and J.K. Norskov, J. Catal. 223 (2004) 232.
[34] B.E. Nieuwenhuys, A.C. Gluhoi, E.D.L. Rienks, C.J. Weststrate and C.P. Vinod, Catal. Today 100 (2005) 49.
[35] L.M. Molina and B. Hammer, Phys. Rev. B 69 (2004) 155424.
[36] L.M. Molina and B. Hammer, Phys. Rev. Lett. 90 (2003) 206102.
[37] G.B. Hoflund, S.D. Gardner, D.R. Schryer, B.T. Upchurch and E.J. Kielin, Appl. Catal. B 6 (1995) 117.
[38] D.A. Outka and R.J. Madix, Surf. Sci. 179 (1987) 351.
[39] D.H. Parker and B.E. Koel, J. Vac. Sci. Technol. A 8 (1990) 2585.
[40] Y. Xu and M. Mavrikakis, J. Phys. Chem. B 107 (2003) 9298.
[41] G. Mills, M.S. Gordon and H. Metiu, J. Chem. Phys. 118 (2003) 4198.
[42] M. Mavrikakis, P. Stoltze and J.K. Norskov, Catal. Lett. 64 (2000) 101.
[43] F. Boccuzzi, A. Chiorino, S. Tsubota and M. Haruta, Catal. Lett. 29 (1994) 225.
[44] I.N. Remediakis, N. Lopez and J.K. Norskov, Angew. Chem. Int. Ed. 44 (2005) 1824.
[45] G.R. Bamwenda, S. Tsubota, T. Nakamura and M. Haruta, Catal. Lett. 44 (1997) 83.
[46] F. Boccuzzi, A. Chiorino, S. Tsubota and M. Haruta, J. Phys. Chem. B 100 (1996) 3625.
[47] Z.-P. Liu, P. Hu and A. Alavi, J. Am. Chem. Soc. 124 (2002) 14770.